Spectroscopy of neutron-rich nickel isotopes: Experimental results and microscopic interpretation

M. Girod
Service de Physique et Techniques Nucléaires, C.E. Bruyeres-le Châtel, Boîte Postale 12, 91680 Bruyeres-Le-Chatel, France

Ph. Dessagne,* M. Bernas, M. Langevin,† F. Pougheon, and P. Roussel
Institut de Physique Nucléaire, Boîte Postale 1, 91406 Orsay Cedex, France
(Received 18 May 1987)

The spectroscopy of neutron-rich isotopes of ^{67}Ni and ^{68}Ni is studied using the quasi-elastic transfer reactions (^{14}C,^{16}O) and (^{14}C,^{17}O) on a ^{70}Zn mass separated target. The structure of these exotic nuclei is investigated in the framework of a microscopic collective model based on the Hartree-Fock-Bogoliubov theory. Gogny's two-body effective interaction is used. Collective excited states of ^{68}Ni are obtained by solving the Bohr Hamiltonian in which inertia parameters are calculated in the cranking approximation. Spin and parity assignments to observed excited levels are suggested on the basis of information deduced from this analysis. This assignment is further checked by comparing measured angular distributions to predictions. Predictions of the level structure of ^{70}Ni and ^{78}Ni isotopes are given. A more precise test of the 0^+ wave functions is provided by the calculation of monopole operator of the $0_1^+ \rightarrow 0_2^+$ transition in ^{68}Ni. An impressive agreement is obtained between the measured and calculated half-life.

I. INTRODUCTION

The nuclear structure calculations reported in this paper are based on the mean field theory and use a two body effective interaction. They are extended here to neutron rich nuclei in the intermediate mass region; thus the effective interaction, calibrated on bulk properties of stable nuclei, will be tested on nuclei far from stability.

Since they have a proton closed shell, heavy isotopes of nickel are good candidates for this test. Interesting properties are expected at the neutron subshell and shell closures when $N=40$ or 50.

The first few states of the new isotopes of ^{67}Ni, ^{68}Ni have been measured by using quasi-elastic transfer reactions (^{14}C,^{16}O) and (^{14}C,^{17}O). Even though the mass excess of ^{68}Ni,[1] the spin and parity assignment,[2] and decay time measurement of the first level in ^{68}Ni (Ref. 3) have been already published, they are recalled and completed here by the study of other exited states in ^{68}Ni and in ^{67}Ni. Altogether, this set of data provide the material to compare with structure calculations developed in the frame of Hartree-Fock-Bogoliubov (HFB) formalism. Starting from the potential energy surfaces as function of the deformations, the inertia parameters are obtained using the cranking approximation. The collective excited states are calculated via the evaluation of the Bohr Hamiltonian for the studied isotopes, and for a few others more neutron rich and not yet measured. Besides their interest in nuclear structure, these nuclei are important to study since they appear at first in the rapid neutron capture process in astrophysics; a knowledge of their properties (mass excess and β decay scheme) is necessary to reproduce natural abundances of heavy nuclei.

In the first section we shall briefly report on properties of ^{67}Ni, ^{68}Ni as they can be deduced from quasi-elastic transfer reactions. The theoretical method is presented with some details and the measured excited states are analyzed in light of the proposed level schemes. The second section concerns the calculation of the monopole strength parameter between the 0^+ states in ^{68}Ni making use of the collective wave function. This type of calculation, performed for the first time, is accounted for.

II. SPECTROSCOPY OF NEUTRON RICH NUCLEI ^{67}Ni, ^{68}Ni

A. Experiment

1. Experimental setup

The 72 MeV, ^{14}C beam was delivered by the Tandem in Orsay with an intensity of $\approx$20 to 50 nA/p. Mass separated target of ^{70}Zn (see Table I) was prepared on a ^{12}C backing by the mass separator "Paris" at the R. Bernas Laboratory. The isotopic purities were better than 1 per 1000, but chemical contaminants (mainly oxygen) were still present, although special attention was paid to handling the targets in an air free atmosphere. The analyzing system consists of a doubly focusing magnetic spectrometer, "Bacchus," equipped with a set of two position sensitive counters followed by a $\Delta E_1 - \Delta E_2 - E$ ionization chamber. This system allows both an accurate momenta and angle ray tracing calculation ($\Delta p/p \approx 10^{-3}$ and $\Delta\theta = 0.2°$) and redundant ion identification. The horizontal angular opening is 5° for a solid angle of 3 msr.[4]

TABLE I. Target thickness.

^{12}C	Backing	25 $\mu g/cm^2$
^{70}Zn	Mass separated	80 $\mu g/cm^2$
^{70}Zn	Enriched to 70%	$\approx$250 $\mu g/cm^2$

2. Spectra

The spectra of the ^{68}Ni and ^{67}Ni isotopes were simultaneously recorded since the ^{16}O and ^{17}O from the (^{14}C, ^{16}O) and (^{14}C, ^{17}O) reactions show a similar magnetic rigidity (Fig. 1). An overall energy resolution of 100 keV is obtained, which comes mostly from target inhomogeneities. Appropriate corrections were made to eliminate the kinematical $B\rho$ dependence upon θ for the reaction of interest.

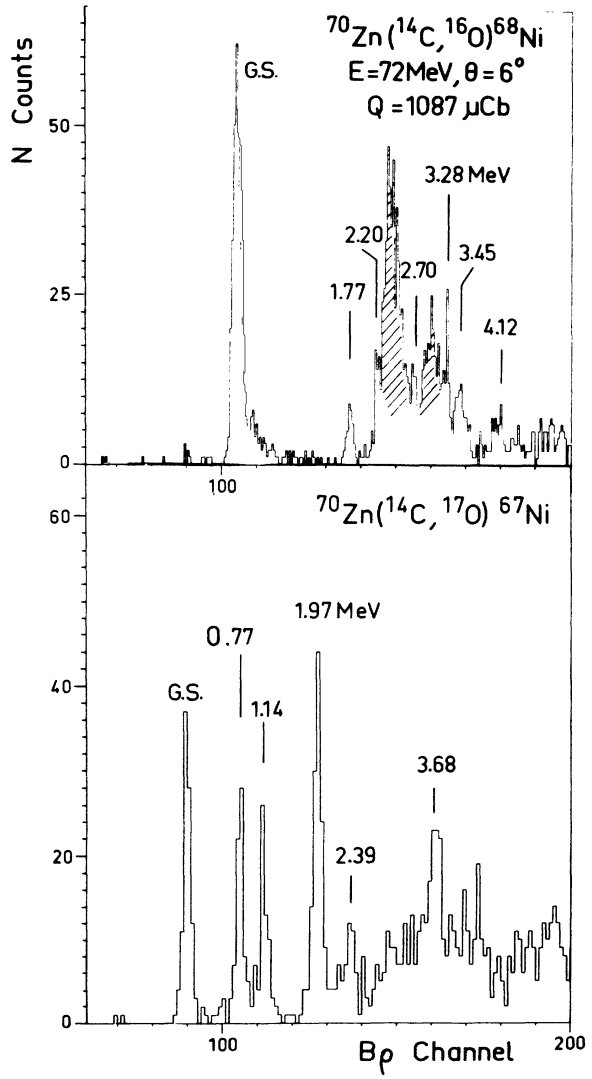

FIG. 1. Spectra of ^{16}O and ^{17}O showing the excited states of ^{68}Ni and ^{67}Ni. The dashed area is due to oxygen target contaminant.

On the ^{67}Ni spectrum, six levels are seen, four of which had been reported previously by Kouzes *et al.* from the $^{70}Zn(^4He, ^7Be)^{67}Ni$ measurement.[5] The ^{67}Ni mass excess presently measured is 64.07±0.10 MeV (Table II) which differs with the value of Kouzes by 0.250 MeV. Furthermore, the excited state energies found here are different from the previous ones. In our case, calibrations in energy are facilitated by the wide energy range ($\Delta E \sim 12$ MeV) of the spectrometer and by the many reaction channels on targets and on contaminants of well known kinematics. Thus even if less accurate, our results are reliable.

For ^{68}Ni, the mass excess is remeasured to be −63.53±0.03 MeV in agreement with the previous result obtained with the (^{18}O, ^{20}Ne) transfer[6]—see Table II—the accuracy is better than for ^{67}Ni because of a larger cross section and a better compatibility of our different measurements. The first excited level is clearly seen at 1.77 MeV±0.03 MeV excitation energy. The other states (Fig. 1) are indeed due to Ni levels, since the backscattered ^{16}O line is clearly identified from its difference in kinematical factor. In these pickup reactions, the energy mismatch hinders the excited levels when excitation energy increases.

The ^{69}Ni isotope was both observed and its mass excess measured for the first time from the $^{70}Zn(^{14}C, ^{15}O)^{69}Ni$ reaction.[7] Only the mass excess could be measured because the cross section, already low for the ground state (3 $\mu b/sr$), is even lower for populating excited states. One of our present aims is a theoretical analysis of the set of results concerning the isotopes of ^{67}Ni, ^{68}Ni mentioned above.

3. Angular distributions

As compared with light ion reactions, heavy ion transfer reactions have been quite disappointing for spin attribution. To obtain similar information, the range of observation should be shifted to very small angles.[8] Therefore, an experimental device has been developed for accurate angular measurements at very forward angles, including 0°. A double series of beam catchers has been set in the vacuum chamber of the spectrometer in order to trap the beam and measure its intensity without intro-

TABLE II. Mass excess and excitation energies of new nuclei.

Nucleus	^{67}Ni		^{68}Ni
Mass excess		−63.74±0.02[a]	−63.47±0.03[b]
		−64.7 ±0.1	−63.53±0.01
		Ref. 5	
Excitation	0.72	0.77±0.03	1.77±0.03
Energies	1.02	1.14	2.20
	1.71	1.97	2.70
		2.39	3.28
		3.68	3.45
			4.12

[a]From Ref. 5.
[b]From Ref. 6.

ducing a prohibitive increase of the background level in the image space of the magnet. A good rejection of the primary beam, better than 10^{13}, is achieved. The appropriate catcher is selected according to the ratio of the magnetic rigidity of the ion of interest, versus that of the incident particles. Measurements were performed from 0° to 15° with a 0.2° angular accuracy.

The $0^+ \rightarrow 0^+$ nuclear transitions involving even-even nuclei are expected to be characterized by strong forward enhancement. This is indeed verified in the case of ground state (g.s.)→g.s. transitions. Since a similar enhancement (by a factor of 6) was observed in the angular distribution of the first excited state of the ^{70}Zn(^{14}C,^{16}O)^{68}Ni* reaction, the spin 0^+ could be assigned to this level. A DWBA calculation was performed in order to compare the shape of the angular distribution for a 0^+ final state and for the more probable case of a 2^+ state. This calculation assumes a direct one step transfer of two protons—(sequential transfer would not change the shape but the normalization factor)—and optical potentials as they are given in Table III.[9] It confirms that indeed the spin 0^+ can be attributed to the first excited level of ^{68}Ni (Fig. 8).

The angular distributions for the other levels of ^{68}Ni were also measured but with a lower accuracy because of the smaller values of cross sections and of the increased level of background. The DWBA analysis was performed for these results, using the same mechanism assumptions and the same optical potentials as before.

This simplified description of the reaction was extended to the case of three nucleon pickup in the ^{70}Zn(^{14}C,^{17}O)^{67}Ni reaction. For an odd A nucleus and for a $\frac{5}{2}^-$ ejectile, many values of the spin transfer are involved and the distribution shapes are not characteristic of the final spin value.

Properties of the final states are proposed on the basis of level schemes obtained from the HFB calculations. The comparison of the measured angular distributions with the calculated DWBA curves is used to test these assumptions. This discussion will come later.

B. The HFB calculations

1. General features

The theoretical description of the structure of these nuclei has been performed in the framework of the Hartree-Fock-Bogoliubov theory. This method permits us to describe bulk nuclear properties in the mean field approximation. The main advantage of microscopic methods lies in that nuclear structure properties are described starting from a unique effective interaction. Neither *a prior* hypothesis nor adjustable parameters are necessary, even for the pairing correlations. In the present calculations the two-body force is the finite range, density dependent, effective interaction D1SA, derived from the Gogny's D1 force.[10] It was adjusted to describe self-consistently the mean field and the pairing field on the same footing. The D1SA effective interaction results from a slight modification of this D1 force, aimed at improving its surface properties,[11] and at reducing the pairing correlations which are consistently produced.

The spectroscopic study of several nuclei, using the D1 force, shows that the spectra obtained from the diagonalization of Bohr Hamiltonian are systematically expanded compared to the experimental ones. The inertia parameters seem to be underestimated. It is partially due to the cranking approximation used for calculating the inertia parameters but it may also arise from an overestimation of the pairing correlations. Actually, the small change made in the pairing properties of the force leads to an important increase of the inertia parameters, and consequently to an improvement of the calculated spectra. In particular, the difference between the calculated moments of inertia and those deduced from the experimental spectra of the "good" rotational nuclei are systematically reduced when using D1SA force.

The pairing correlations were diminished so that the experimental odd-even binding energy differences between adjacent nuclei could be reproduced—at the HFB approximation—using the tin isotopes as a test. Indeed, when adjusting the D1 force,[10] these binding energy differences were intentionally overestimated because, in odd nuclei, the explicit treatment of the quasiparticle vibration coupling would reduce these differences.[12] Therefore, one may consider that this coupling has been simulated by fixing the D1SA force. This has been achieved without significantly changing the nuclear matter properties of the D1 force. Moreover, the results shown in Ref. 10 for the magic nuclei are not modified when using the D1SA force. Altogether this interaction is expected to give reasonable predictions for exotic nuclei.

2. The collective dynamics

As a matter of fact, the HFB wave function is a Slater determinant which, in general, is not appropriate to describe the ground and excited states of a nucleus. For a complete description of the nucleus, we must generate a dynamical state ψ of the system. In the generator coordinate method, this state ψ can be expressed as a superposition of HFB wave functions ϕ describing the nucleus at different deformations labeled by q:

$$|\psi\rangle = \int \chi(q)\phi_q dq \ , \tag{1}$$

where $\chi(q)$ is a weight function containing the collective

TABLE III. Optical potentials.

	V_{MeV}	$a_v f$	$r_v f$	W_{MeV}	$a_w f$	$r_w f$	$r_c f$
Incident channel ^{14}C	37	0.404	1.35	78	0.174	1.29	1.35
Outgoing channel ^{16}O and ^{17}O	37	0.404	1.35	78	0.174	1.29	1.35

dynamics. With this definition of ψ, the collective wave functions $\chi(q)$ determined through a variational principle, are governed by the Griffin-Hill-Wheeler equations.[13] Because of their complexity, we have not tried to solve these equations directly. Instead, we have made use of an approximate treatment which consists in developing the Hamiltonian and overlap kernels on the nonlocality. This expression leads to an equation of Bohr type:

$$\left[-\frac{\hbar^2}{2}\frac{\partial}{\partial q}\frac{1}{M}\frac{\partial}{\partial q}+V(q)-E\right]\tilde{\chi}(q)=0 \ . \tag{2}$$

Here, $\tilde{\chi}(q)$ is a collective wave function from which the weight function $\chi(q)$ can be derived. M is the collective mass and $V(q)$ is the collective potential which is expressed as

$$V(q)=\langle\phi_q \mid H \mid \phi_q\rangle-\Delta E_q \ . \tag{3}$$

The first term in Eq. (3) is the HFB energy $E(q)$, while the second one is the zero-point-energy correction coming from the fluctuation of the collective variables in the HFB states.[14] This term and the collective masses are derived in the framework of the cranking model.[15]

The adiabatic approximation is involved in the following assumption: the total wave function is a product of an intrinsic state with a collective wave function. This has been assumed for the derivation of a Bohr-type Hamiltonian from the Hill-Wheeler equations. The Bohr Hamiltonian is a pure collective Hamiltonian where the microscopic HFB wave function do not appear explicitly.

For the description of the low energy rotational and vibrational spectra, the general form of the Bohr Hamiltonian is[16]

$$H=V(\beta_0,\beta_2)+\frac{1}{2}\left[B_{00}(\beta_0,\beta_2)\dot{\beta}_0^2+2B_{02}(\beta_0,\beta_2)\dot{\beta}_0\dot{\beta}_2+B_{zz}(\beta_0,\beta_2)\dot{\beta}_2^2+\sum_k\frac{\langle I_k^{2r}\rangle}{J_k(\beta_0,\beta_2)}\right], \tag{4}$$

where V is the triaxial collective potential defined in Eq. (3), $B_{mn}J_k$ the inertia parameters for the vibrations and rotations, and k corresponds to the three intrinsic axes. The collective variables β_0 and β_2, the shape variables, are related to the expectation values of the quadrupole operators $Q_0\sim r^2Y_{20}$ and $Q_2\sim r^2(Y_{22}+Y_{2-2})$. In this collective space the total wave function has the explicit form

$$\psi_{nI}(x)=\int\sum_K\Phi^I_{nK}(\Omega)\tilde{\chi}_{nIK}(\beta_0,\beta_2)\phi(\beta_0,\beta_2,x_i)d\Omega\,d\tau \ , \tag{5}$$

with

$$d\tau=[(B_{00}B_{22}-B_{02}^2)J_xJ_yJ_z]^{1/2}d\beta_0 d\beta_2 \ , \tag{6}$$

where K is the projection of the total angular momentum I on the intrinsic z axis, and Φ is the symmetrized rotational function depending upon the three Euler angles Ω between the laboratory and the intrinsic axes. The HFB wave functions ϕ are related to the nucleon coordinates x_i $(i=1,A)$, as well as to the shape variables. Note that ϕ does not depend explicitly upon I or K (adiabatic approximation). The Bohr Hamiltonian is determined completely by seven functions of β_0 and β_2, namely the collective potential V and the six inertial functions: B_{00}, B_{02}, B_{22}, J_x, J_y, J_z. The calculation of these seven functions at different deformations is performed through a constrained HFB method. An important feature of this model is that all the ingredients of Eq. (4) can be calculated from the self-consistent HFB approach.

3. *Constrained HFB method and inertial functions*

To generate the microscopic HFB wave functions, the HFB method with external fields is used.[17] The equations are obtained by a minimization of the total energy

$$\delta(\langle\phi\mid\hat{H}_{\rm eff}-\lambda_Z\hat{Z}-\lambda_N\hat{N}-\mu_0\hat{Q}_0-\mu_2\hat{Q}_2\mid\phi\rangle)=0 \ , \tag{7}$$

and the constraint conditions

$$\begin{aligned}&\langle\phi\mid\hat{Z}\mid\phi\rangle=Z \ ,\\ &\langle\phi\mid\hat{N}\mid\phi\rangle=N \ ,\\ &\langle\phi\mid\hat{Q}_i\mid\phi\rangle=q_i \ ,\end{aligned} \tag{8}$$

where $H_{\rm eff}$ is the nuclear effective Hamiltonian and λ and μ are Lagrange multipliers. The first two conditions ensure that the average number of protons and neutrons is conserved while the other ones prescribe triaxial deformations characterized by q_0 and q_2. The calculation of the HFB energy E with respect to the intensity of the external fields Q_0 and Q_2 generate the so-called potential energy surface (PES), that is $E(q_0,q_2)$. The inertia parameters are calculated in the cranking approximation.[15]

The stability of the value of the inertia parameters versus the size of the oscillator basis chosen to develop HFB wave functions has been tested. These parameters are found to decrease smoothly in magnitude when N, number of major shells, is increased. From $N=7$ to $N=11$, they decrease by less than 15%.

C. Results

1. *Potential energy surfaces*

We have calculated the potential energy surface for the ^{68}Ni nucleus. The unknown isotopes of ^{70}Ni and ^{78}Ni have been calculated also in order to anticipate their properties. These collective potentials shown in Figs. 2 and 3 are defined in terms of the traditional parameters β and γ which are related to β_0 and β_2 via $\beta_0=\beta\cos\gamma$ and $\beta_2=\beta\sin\gamma$. The potential for ^{78}Ni indicates that this nucleus is spherical and very rigid against β deformation. This is not a surprise, since this nucleus has a neutron full shell at $N=50$. The potentials for ^{68}Ni and ^{79}Ni also display a spherical minimum, but for ^{68}Ni, a second minimum exists near the deformation $\beta=0.3$. This minimum could corresponds to a 0_2^+ deformed isomeric state. This very interesting situation will be discussed later in the context of experimental results (i.e., spin and

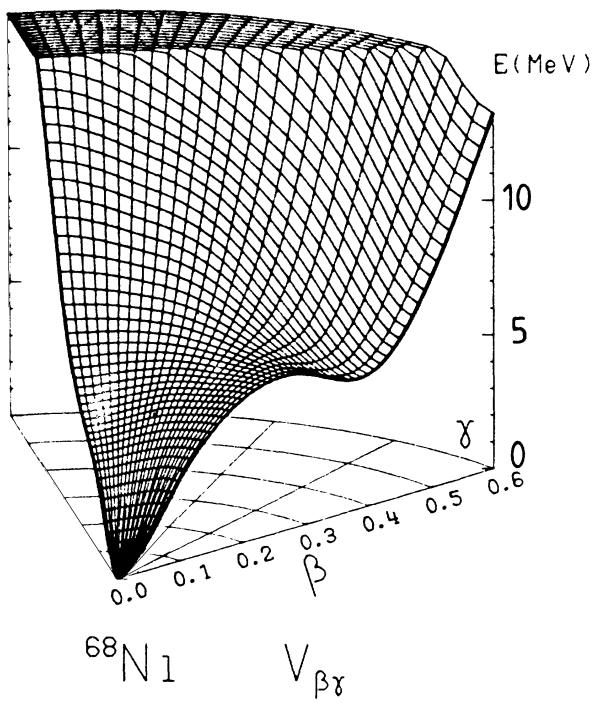

FIG. 2. Triaxial deformation energy surface calculated for ^{68}Ni represented in the $\beta-\gamma$ space.

parity as well as half-life) obtained for this state.

Figure 4 shows the potential energy surface $V(\beta,\gamma=0°$ and 60°) for Ni isotopes from $A=68$ until $A=78$ as function of the β deformation. Between the quasimagic nucleus ^{68}Ni and the doubly magic nucleus ^{78}Ni, the intermediate nuclei are more or less soft around a spherical shape. In addition, in Fig. 5 we have reported the two-neutron separation energy of these isotopes presently calculated and for sake of comparison, their value according to the predictions of Uno and Yamada[18] and Möller and Nix.[19]

2. *Theoretical results: Comparison with the data*

A numerical calculation of the Bohr Hamiltonian was performed using the code of Kumar.[16,20] The excited states obtained from this diagonalization can be compared with the experimental results or can lead to some predictions for yet unknown nuclei. Due to chosen symmetries of the Bohr Hamiltonian, only the rotational-vibrational states with positive parity could be obtained with this method.

The diagonalization of the Bohr Hamiltonian gives also the wave functions of the collective levels which are interpreted as deformation probability amplitudes for the states in the collective space $\beta-\gamma$. The calculated level scheme of ^{68}Ni is compared with measured results in Fig. 6.

^{68}Ni nucleus. The energies of the first 0^+ and 2^+ excited levels are reproduced well enough by the theory. An interpretation of the first two 0^+ levels can be suggested by the dynamical description. The structure of the potential energy surface of ^{68}Ni reported in Figs. 2–4 allows one to relate the ground state to the spherical state, and the second 0^+ to the deformed minimum. However, the potential energy surface alone cannot provide a definitive conclusion, since the contribution of the collective inertia parameters are important, particularly the vibrational masses. The calculation shows that the mass-parameter

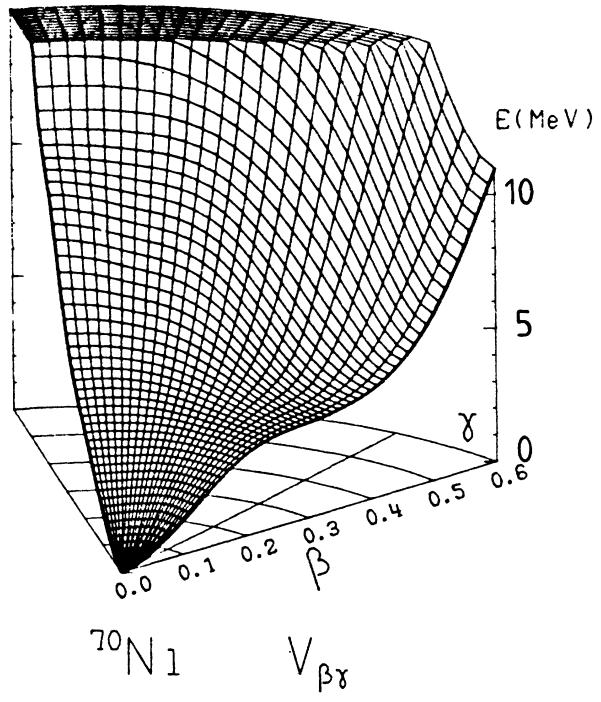

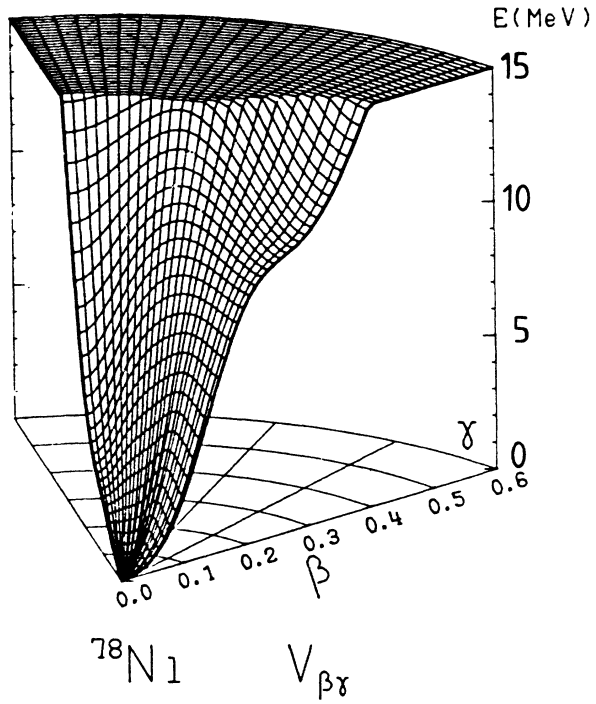

FIG. 3. Triaxial deformation energy surface calculated for ^{70}Ni and ^{78}Ni represented in the $\beta-\gamma$ space.

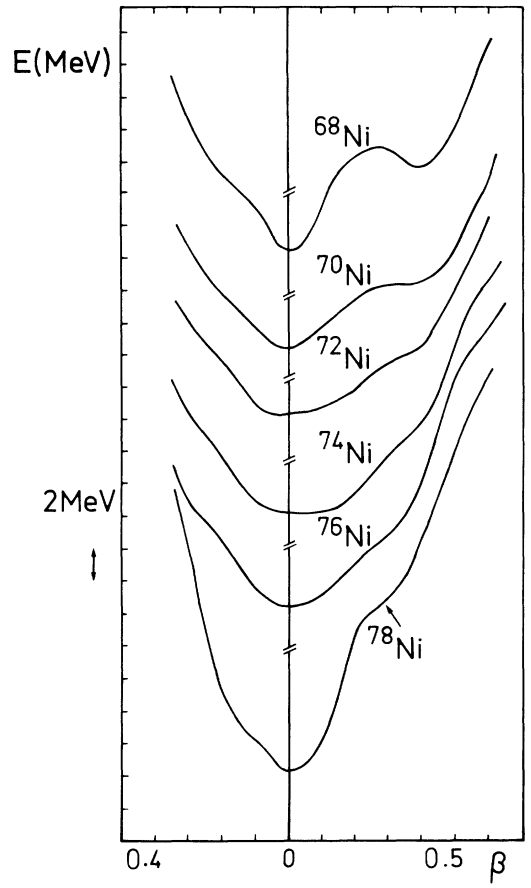

FIG. 4. Axial deformation energy curve calculated for the series of even Ni isotopes with $A=68$ to $A=78$.

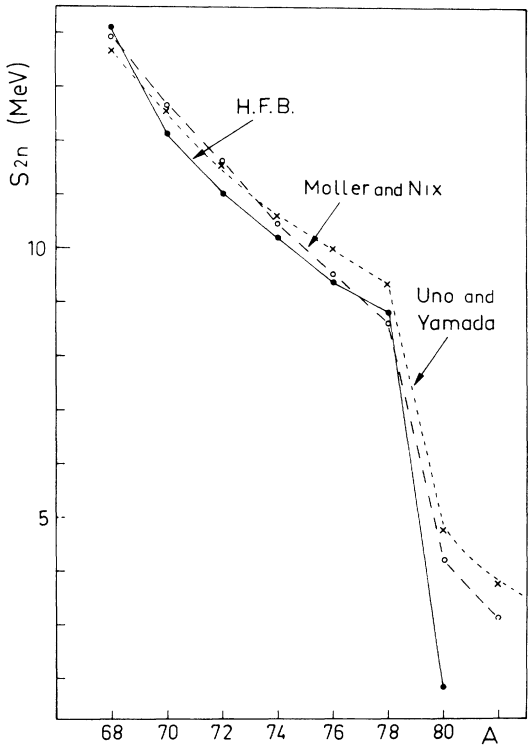

FIG. 5. $2n$ separation energy of even Ni isotopes: Comparison between the present HFB calculations and the results of Uno and Yamada (Ref. 19) and Möller and Nix (Ref. 20).

B_{00} is minimum for $\beta=0$ and maximum near $\beta=0.3$. This mass parameter governs the zero-point energy, i.e., the energy of the first 0^+ with respect to the minimum of the potential energy surface. With the zero-point energy found here, the 0_2^+ level is located about 500 KeV above the minimum of the deformed well, below but near the top of the barrier between the two minima (Fig. 4).

The first 0^+ wave function (Fig. 7) peaks near the spherical point while the second 0^+ wave function displays two peaks: the first one is located near $\beta=0$, and the second one, larger in magnitude, is maximum near $\beta=0.3$. This wave function is in fact spreading over the first (spherical) and the second (deformed) minima of the potential energy surface (Fig. 2). Therefore, it is sensible to interpret this 0_2^+ level as a shape isomeric state. Other collective levels are reported in Fig. 6 together with measured ones. The DWBA analysis was performed for the measured states with the same mechanism assumptions and same optical potentials (Fig. 8 and Table III). Quantum numbers of the final states were assumed from the level scheme resulting from the HFB calculations.

Both shape agreement and normalizing factors bring information on the likelihood of the quantum numbers. For the first three states, the spin assignment is not ambiguous. For the two following states, two spin values were guessed for each case; the best fit is obtained with 0^+ and 2^+ for the levels at 2.70 and 3.28 MeV, respectively. The normalization factor $N=(d\sigma/d\Omega_{\text{exp}})/(d\sigma/d\Omega_{\text{DWBA}})$ shown in Table IV also indicates small spin values. In this reaction the angular momentum matching enhances small spin states. Spin assignment is not attempted for the two last states identified at 3.45 and 4.12 MeV, since

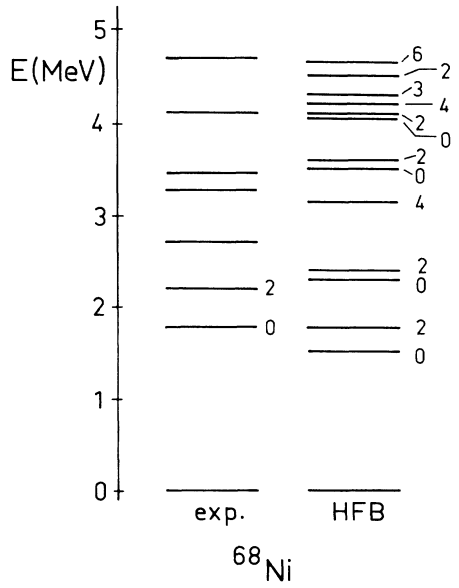

FIG. 6. Collective levels (natural parities) of ^{68}Ni compared with experimental data.

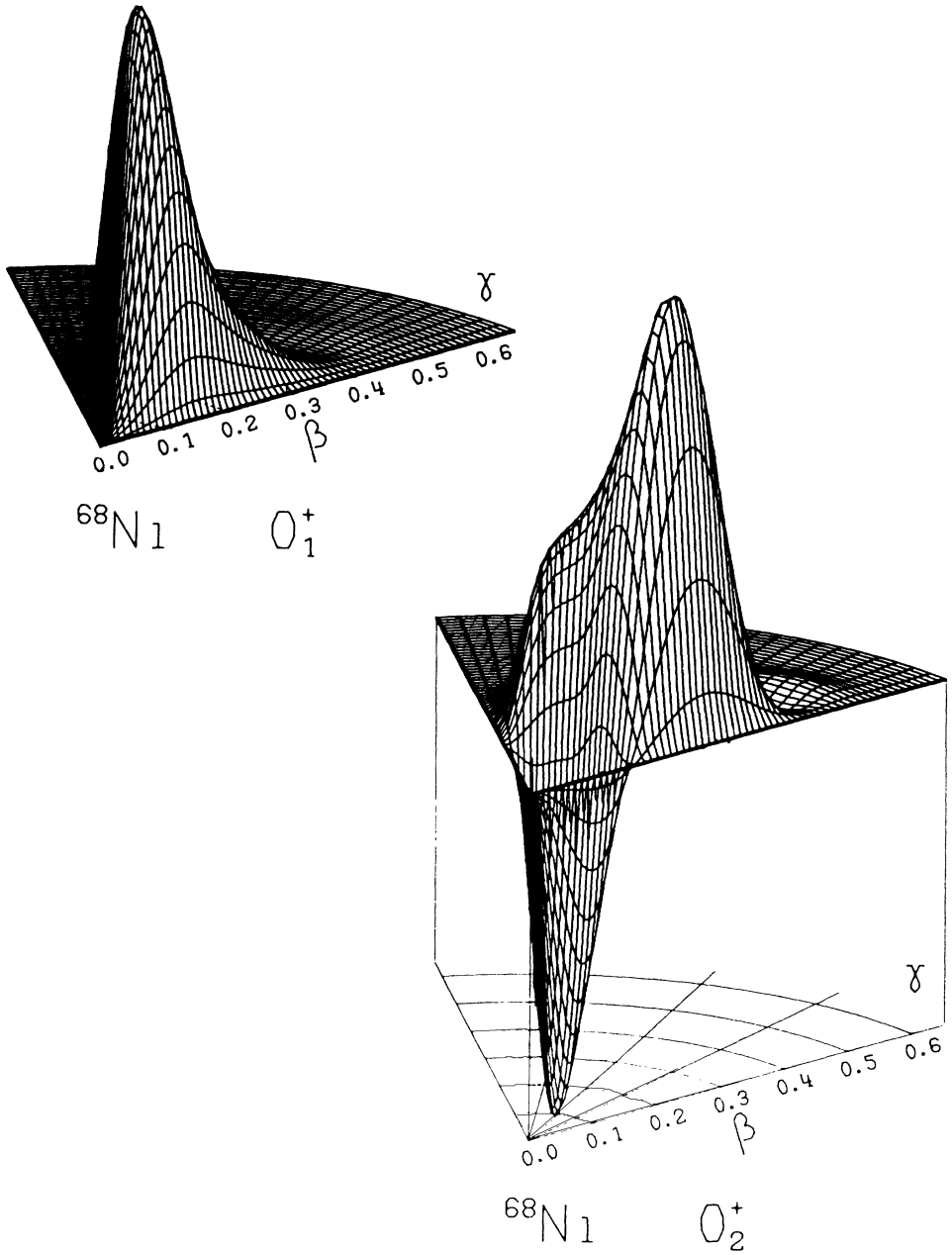

FIG. 7. Collective wave functions of the two 0^+ first levels of ^{68}Ni represented in $\beta-\gamma$ space. Note that the five-dimensional metric [Eq. (6)] which has been included here, makes the wave functions vanishing on the axis $\gamma=0°$ and 60°.

the structures in the angular distributions vanish. Even though the reaction mechanism description given with DWBA is not appropriate for using the HFB wave functions, the ratio of the cross sections leading to the first two 0^+ states was estimated from the occupation numbers given by the HFB calculations. In a very approximate way, the two 0^+ wave functions may be written as two orthonormalized configurations for the g.s. and the 1st excited as follows:

$$|0_1^+\rangle = a\,|(p_{1/2})^2\rangle + b\,|(g_{9/2})^2\rangle\ ,$$

and

$$|0_2^+\rangle = -b\,|(p_{1/2})^2\rangle + a\,|(g_{9/2})^2\rangle$$

with $a^2=b^2=1$ and $a\simeq 0.85$ and $b\simeq 0.52$.

Assuming that in the ^{70}Zn nucleus the neutrons mostly fill the $p_{1/2}$ states with only a negligible $g_{9/2}$ component, then to first order, the ratio of observed cross sections should be

$$\frac{(d\sigma/d\Omega)_{0_1^+}}{(d\sigma/d\Omega)_{0_2^+}} \approx a^2/b^2 \approx 2.67\ ,$$

which is indeed similar to the measured ratio of 3.08 (see

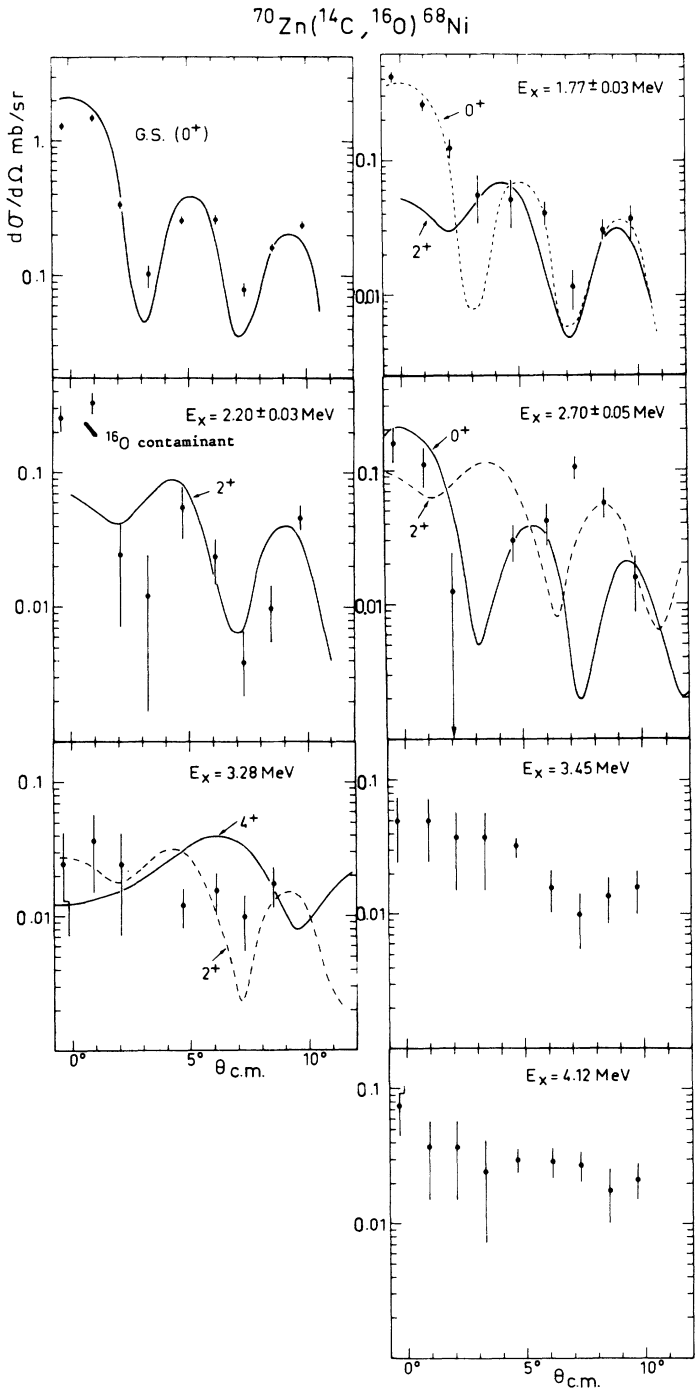

FIG. 8. Angular distributions for the set of levels observed in Ni isotopes: Present measurements and DWBA calculations.

Table IV). In order to further test the 0^+ calculated wave functions, the $0_2^+ \rightarrow 0_1^+$ decay rate in ^{68}Ni was measured. The relevant calculation is detailed in the next section. Predictions concerning the ^{70}Ni and ^{78}Ni level scheme are also presented in Fig. 9 prior to experiment.

^{67}Ni nucleus. A dynamical calculation for ^{67}Ni was not performed, but instead, the blocking procedure was adopted. This method is designed to describe the first particle-hole excitations in even-odd nuclei.[10] The calculation was performed as follows: On an even-even core (^{66}Ni) a quasiparticle state is created and then the total energy functional is minimized with this new trial wave function. This minimization was realized with different blocked quasiparticle states close to the Fermi surface, assuming the spherical symmetry. The blocked state which leads to the lowest energy in the minimization procedure is associated with the g.s. of the even-odd nucleus and the following blocked states describe the first low-lying excited states. The spin and parity assignment of the levels is given by the spin and parity of the blocked

TABLE IV. Observed states in ^{68}Ni and ^{67}Ni with their assumed spin and parities. The normalizing factor N is the ratio $d\sigma/d\Omega_{exp}/d\sigma/d\Omega_{DWBA}$.

^{68}Ni			^{67}Ni		
Excitation energy (MeV)	Spin	N	Excitation energy (MeV)	Spin	N
g.s.	0^+	0.4	g.s.	$(\frac{1}{2}^-)$	0.37
1.77±0.3	0^+	0.13	0.77±0.2	$\frac{9}{2}^+$	2.93
				$\frac{5}{2}^+$	2.35
2.20±0.4	2^+	0.21	1.14±0.03	$\frac{3}{2}^-$	0.20
2.70±0.04	0^+	0.1	1.97±0.04	$\frac{3}{2}^-$	1
	2^+	0.5			
3.28±0.05	2^+	0.2	3.68±0.05	$\frac{3}{2}^-$	1.1
	4^+	1.43			
3.45±0.05					
4.12±0.05					

single-particle states. Such a method was already applied to the ^{73}Zn nuclei.[21] The results of this calculation for ^{67}Ni is illustrated in Fig. 10. The first two levels are found separated by only 260 keV. Given that the blocking procedure is an approximation (since the quasiparticle vibrational coupling which can induce a level shift, is neglected) one can only conclude that the ^{67}Ni g.s. is either $\frac{1}{2}^-$ or $\frac{5}{2}^-$. In order to evaluate the level of confidence associated to our calculated scheme, the blocking calculation was also performed for ^{65}Ni. The first two levels are found to be very close in energy, as known from experiment,[22] but inverted. The calculated spectrum of ^{69}Ni is also shown prior to experiment.

Although the assumption of a direct pickup of a three-nucleon cluster is questionable, we have used it to calculate angular distributions of the (^{14}C, ^{17}O) transfer reaction. The quality of the fit (Fig. 11) and the value of the normalizing factor defined as before (Table IV) provides arguments on possible spin values of the ^{67}Ni states. The g.s. is assumed to be $\frac{1}{2}^-$ on the basis of its $\beta-\gamma$ decay scheme.[23] This is consistent with the shape of the angular distribution. The occurrence of a $\frac{5}{2}^-$ state, at very low excitation energy, is possibly hidden, since this level may be too close to the g.s. or its cross section may be smaller than for a $\frac{1}{2}^-$ state. The first excited state is likely to be $\frac{9}{2}^+$ although the cross section is larger than expected. The three other states might be $\frac{3}{2}^-$, but the shape of the angular distributions are not characteristic.

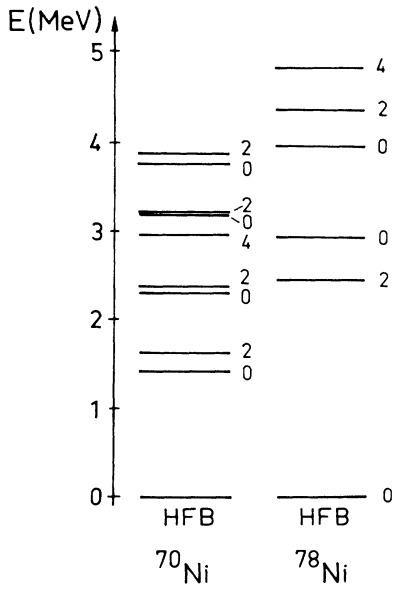

FIG. 9. Predicted collective levels of the unknown isotopes of ^{70}Ni and ^{78}Ni.

III. THE MONOPOLE DECAY OF THE 0^+ LEVEL IN ^{68}Ni

A series of light or medium mass nuclei have a 0^+ as first excited state, i.e., ^{16}O, ^{40}Ca, ^{72}Ge, ^{90}Zr, ^{96}Zr, and ^{98}Mo. The structure of these 0_2^+ states shows enhanced symmetries and collective properties. The new isotope of ^{68}Ni is similar to ^{90}Zr since 40 nucleus are associated with 28 or 50 complementary nucleons, respectively, which are both magic numbers. Beyond $N=40$, from the classical shell model, the next subshell is the $g_{9/2}$. Then the two quasiparticle excitation energy is reduced by the stronger coupling of a nucleon pair occurring on this subshell. The Nilson neutron diagram calculated for ^{68}Ni, with the HFB method, is reported in Fig. 12. At spherical point, the 40 neutrons fill the successive subshells up to $2p_{1/2}$. When a small deformation enters, due to some collective excitation, the last pair of neutrons may shift to the $g_{9/2}$ subshell (on the $\frac{1}{2}^+$ or the $\frac{3}{2}^+$ orbital) in order to minimize the overall energy of the nucleus. The occupation numbers are given which indicate the behavior of the nucleus as a function of its deformation. The half-life $\tau_{1/2}$ of the first 0^+ excited state of ^{68}Ni has been derived from the measurement of time delayed coincidences between the ^{16}O emerging from the ^{70}Zn(^{14}C, ^{16}O)^{68}Ni(0_2^+) reaction and the electron associated with the ^{68}Ni(0_2^+) de-

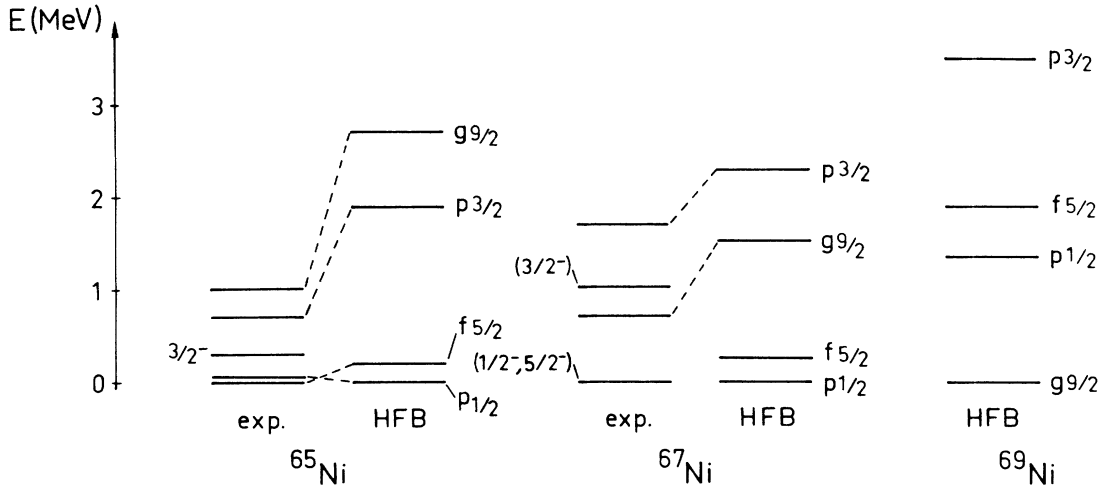

FIG. 10. Comparison of calculated levels of the odd ^{65}Ni and ^{67}Ni isotopes with data. Calculated level scheme for ^{69}Ni.

cay.[3] The value for the half-life $\tau_{1/2}=211\pm^{60}_{40}$ ns is related to the monopole strength with good accuracy since the atomic aspect of the decay is well accounted for.[24]

The absolute transition probability $W=1/\tau$ may be written as the product of an electronic factor Ω, almost independent of the nuclear states involved in the decay, and the square of the nuclear "strength parameter" ρ, independent of the atomic process:

$$W=\Omega\rho^2 .$$

The factor Ω can be decomposed as a sum of two terms: Ω_e is the electron transition probability which takes place between the $K(L,M)$ atomic shell, towards the continuum state, and Ω_π is the formation of an electron pair (e^+,e^-):

$$\Omega=\Omega_e+\Omega_\pi .$$

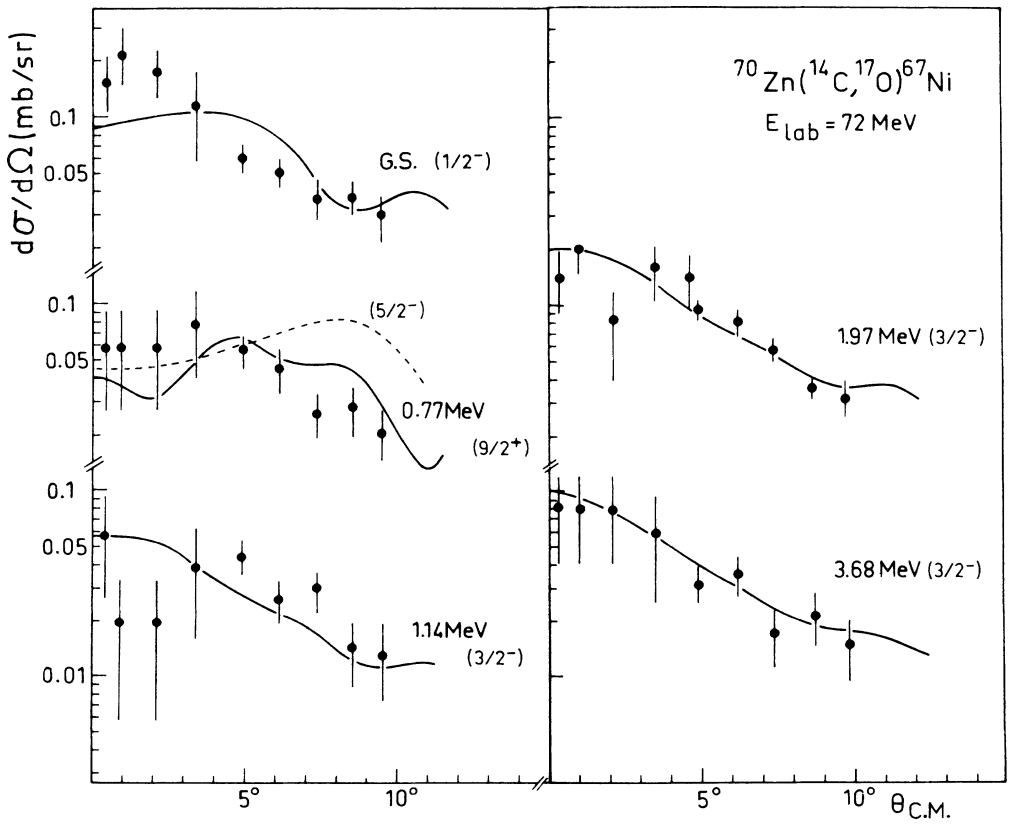

FIG. 11. Angular distributions of the levels observed in ^{67}Ni: Present measurements and DWBA calculations.

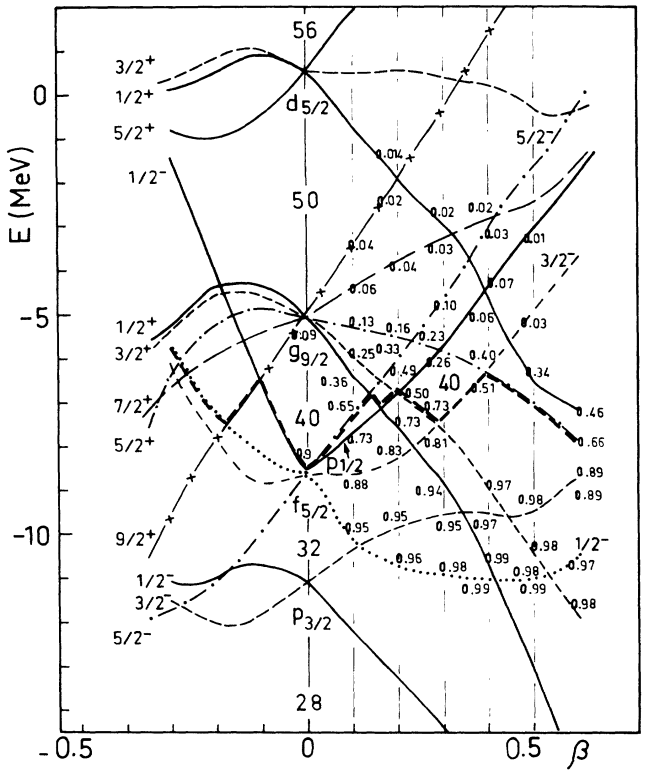

FIG. 12. Neutron HFB single-particle spectra as function of the β parameter. Occupation numbers are reported for each decimal value of the β parameter.

TABLE V. Atomic parameters for the decay of ^{68}Ni-0_2^+ level.

^{68}Ni-0_2^+ level $E=1.77$ MeV
Ω_k (s^{-1}) $=1.85\times10^8$
$\Omega_e/\Omega_k=1.126$
$\Omega_e/\Omega_\pi=0.576$

Using the work of Church and Weneser[25] one finds $\Omega_e=1.126\Omega_K$. In the case of the Ni isotopes, Ω_π and Ω_K have been calculated[25] as a function of excitation energy of the transition and their values are shown in Table V.

The strength parameter ρ is calculated as $\sqrt{W/\Omega}=\pm0.076\pm0.010$. It is related to the transition probability between the two 0^+ states, and thus

$$\rho=\sum_p \int \phi_f^* \left[\left[\frac{r_p}{R} \right]^2 - \sigma \left[\frac{r_p}{R} \right]^4 \cdots \right] \phi_i \cdot dr \ ,$$

where ϕ_i and ϕ_f are, respectively, the initial and final nuclear wave functions, r_p is the position coordinate of the pth proton, and R is the nuclear radii with respect to the proton distribution.

In most cases, the value of σ is smaller than 0.1 (Ref. 25); therefore, only the first term of the development is considered in actual calculations.

The structure of both 0^+ wave functions will play a crucial role for the calculation of the ρ parameter, especially for the matrix element:

$$\int \tilde{\chi}_{100}(\beta_0',\beta_2') \langle \phi(\beta_0',\beta_2',x') \mid \mathbb{R}^\dagger(\Omega') \sum_i r_i^2 \mathbb{R}(\Omega) \mid \phi(\beta_0,\beta_2,x) \rangle \tilde{\chi}_{200}(\beta_0,\beta_2) d\tau\, d\tau' d\Omega\, d\Omega' \ . \tag{9}$$

The collective wave functions of 0^+ levels are invariant under rotations, in contrast with the symmetry properties of the HFB wave functions. This is why the complete evaluation of this matrix element is quite involved since it requires the projection of the HFB wave functions on the angular momentum. It has not been performed, but instead, the rotational model approximation has been invoked for simplicity. It consists of setting the angular overlap equal to $\delta(\Omega-\Omega')$. This is justified since the 0_2^+ level is a well deformed state.[26] It is clear though that this δ approximation cannot be applied to the $(q_0 q_2)$ variables because the two 0^+ wave functions are peaked at very different deformations (see Fig. 7).

After angular integration, we obtain for Eq. (9)

$$\int \tilde{\chi}_{100}(\beta_0',\beta_2') \langle \phi(\beta_0',\beta_2',x') \left| \sum_i r_i^2 \right| \phi(\beta_0,\beta_2,x) \rangle \tilde{\chi}_{200}(\beta_0,\beta_2) d\tau\, d\tau' \ . \tag{10}$$

The matrix elements appearing in Eq. (10) have been calculated by using the many body techniques developed to evaluate matrix elements of one body operator with nonorthogonal HFB wave functions.[27] The calculation of Eq. (10) requires that the domain of integration over the (q_0,q_2) variables be carefully defined. It is well known that in the $(\beta\gamma)$ space describing any triaxial shape, all the possible intrinsic shapes can be represented in the first sextant $\gamma=(0,60°)$. This feature results from the invariance under different ways of labeling or orienting the intrinsic axes with respect to the laboratory axes.[16] However, the first sextant does not represent the whole domain of integration for Eq. (10) since nonzero values of the overlap between the first sextant and the five other ones are involved. Therefore, we have to integrate in the whole $\beta\gamma$ plane from $\gamma=0°$ to 360°. Fortunately, it is not necessary to perform HFB calculations in all the sextants, because the triaxial symmetry permits deduction of all the HFB wave functions, starting from those calculated in the first sextant. A similar consideration allows us to deduce the collective wave functions $\tilde{\chi}_{\text{nik}}$.

In any case, the evaluation of the integrand in Eq. (10) requires the calculation of a large number of matrix elements, typically several thousand, depending on the

(q_0, q_2) mesh size adopted for the numerical integrations. Finally, the integrations have been performed using the two-dimensional Simpson's method developed by K. Kumar on a triangular mesh.

A value of 0.1075 is obtained for ρ, with a calculated value of $R = 15.26$ fm^2. The theoretical value of the half-life of the 0_2^+ level of ^{68}Ni using Eq. (10) is $\tau = 152$ ns. Taking into account that this calculation is fully microscopic and does not contain any adjustable parameters (once the nuclear interaction is fixed), the agreement with the experimental value of 211 ns$^{+60}_{-40}$ is very impressive.

This result shows that the microscopic methods based on the mean field approximation are now able to provide predictions in reasonable agreement with experimental quantities; for instance, the half-life of an excited level which is very sensitive to details of the nuclear dynamics.

The theoretical results presently obtained for exotic nuclei give some confidence in our prediction concerning the more neutron rich isotopes which will be studied in the future.

IV. CONCLUSION

This paper reports and summarizes the experimental results obtained recently on the nuclei ^{67}Ni, ^{68}Ni and uses these results as a test ground for the mean field theory. Excited state energies and angular distributions measured for the (^{14}C, ^{16}O) and (^{14}C, ^{17}O) transfer reactions on ^{70}Zn target and the monopole transition between the first excited state 0^+ in ^{68}Ni and the ground state have been used to test the HFB method of calculation.

Our theoretical analysis of the even-even nuclei has been conducted as follows. In the first stage, the HFB calculation of the potential energy surface was performed, which provides the static properties of the nuclei. The cranking model was used to determine the inertia parameters which are needed to calculate the nuclear dynamics. Finally, the dynamical properties of the nuclei—collective wave functions and excitation energies of the levels—were deduced from a numerical diagonalization of the full Bohr Hamiltonian, which is appropriate to describe low-lying collective states. The results agree well with the measured scheme of even-even nuclei. For even-odd nuclei the blocking procedure provides a reasonable description of the level sequence of ^{67}Ni.

For the magic nucleus of ^{68}Ni we have shown that the first 0^+ excited state is most likely to be a shape isomer. The close correspondence between the measured and the calculated values of the half-life is remarkable considering the absence of any free parameters.

This good overall agreement indicates that the method and the D1SA effective interaction are reliable for mean field theory calculations. On the basis of these results, one might expect to get reliable information on the structure of ^{69}Ni, ^{70}Ni and of the doubly magic ^{78}Ni nucleus, for which predictions are given here, prior to experiment. New experimental ways have to be developed to further investigate these species and check those predictions. Finally, the success of our calculations is largely due to the full self-consistent and realistic description of the nuclear dynamics.

We gratefully acknowledge the assistance of J. F. Berger in helping to derive some of the formulas, the help of I. M. Turkiewicz, E. Quiniou, and G. Parrot at different stages of the experiment, and to M. S. Weiss for rereading the manuscript.

*Permanent address: Centre de Recherche de Strasbourg, Boîte Postale 20, 67037 Strasbourg Cédex, France.

†Deceased.

[1] M. Bernas, J. C. Peng, H. Doubre, M. Langevin, M. J. Levine, F. Pougheon, and P. Roussel, Phys. Rev. C **24**, 756 (1981).

[2] M. Bernas, Ph. Dessagne, M. Langevin, J. Payet, F. Pougheon, and P. Roussel, Phys. Lett. B **113**, 279 (1982).

[3] M. Bernas, Ph. Dessagne, M. Langevin, G. Parrot, F. Pougheon, E. Quiniou, and P. Roussel, J. Phys. (Paris) Lett. **45**, 851 (1984).

[4] P. Roussel, M. Bernas, F. Diaf, F. Naulin, F. Pougheon, G. Rotbard, and M. Roy-Stephan, Nucl. Instrum. Methods **153**, 111 (1978).

[5] R. T. Kouzes, P. Mueller, and C. Yu, Phys. Rev. C **18**, 1577 (1978).

[6] T. S. Bhatia, H. Hafner, R. Haupt, R. Maschuw, and G. J. Wagner, Z. Phys. A **281**, 65 (1977).

[7] Ph. Dessagne, M. Bernas, M. Langevin, G. C. Morrison, J. Payet, F. Pougheon, and P. Roussel, Nucl. Phys. **A426**, 399 (1984).

[8] P. Roussel, J. Phys. (Paris) Colloq. **41**, C3-4, 129 (1980).

[9] J. B. Erskine, W. Henning, D. G. Kovar, L. R. Greenwood, and R. M. Devries, Phys. Rev. Lett. **34**, 680 (1975).

[10] J. Decharge and D. Gogny, Phys. Rev. C **21**, 1568 (1980); M. Girod and D. Gogny, Phys. Lett. B **64**, 5 (1976); M. Girod and P. G. Reinhard, Nucl. Phys. **A384**, 179 (1982); J. Decharge and L. Sips, *ibid.* **A407**, 1(1983).

[11] J. F. Berger, M. Girod, and D. Gogny, Nucl. Phys. **A428**, 23c (1984); L. M. Robledo, J. L. Egido, J. F. Berger, and M. Girod, Phys. Lett. B **187**, 223 (1987).

[12] T. T. S. Kuo, E. U. Baranger, and M. Baranger, Nucl. Phys. **79**, 513 (1966).

[13] D. L. Hill and J. A. Wheeler, Phys. Rev. **89**, 1102 (1953); J. J. Griffin and J. A. Wheeler, *ibid.* **108**, 311 (1957).

[14] M. Girod and B. Grammaticos, Nucl. Phys. **A330**, 40 (1979).

[15] D. R. Inglis, Phys. Rev. **103**, 1786 (1956).

[16] K. Kumar and M. Baranger, Nucl. Phys. **A92**, 608 (1967).

[17] M. Girod and B. Grammaticos, Phys. Rev. C **27**, 2317 (1983).

[18] M. Uno and M. Yamada, Institute for Nuclear Study, University of Tokyo Report NUMA 40, 1982 (unpublished).

[19] P. Moller and J. R. Nix, At. Data Nucl. Data Tables **26**, 165 (1981).

[20] K. Kumar, Prog. Part. Nucl. Phys. **9**, 233 (1983).

[21] M. Bernas, Ph. Dessagne, M. Langevin, J. Payet, F. Pougheon, P. Roussel, W. D. Schmidt-Ott, P. Tidemand-Petersson, and M. Girod, Nucl. Phys. **A413**, 363 (1984).

[22] C. M. Lederer and V. S. Shirley, *Table of Isotopes*, 7th ed. (Wiley, New York, 1978).

[23]E. R. Unite, W. D. Schmidt-Ott, P. Tidemand-Petersson, R. Kirchner, O. Klepper, W. Kurcewicz, E. Roeckl, N. Kaffrell, P. Peuser, K. Rykaczewski, M. Bernas, Ph. Dessagne, and M. Langevin, Nucl. Phys. **A399**, 163 (1983).
[24]A. Passoja, Ph.D. thesis, Jyväskylä, Finland, 1980.
[25]E. L. Church and J. Weneser, Phys. Rev. **103**, 1035 (1956).
[26]A. Zaringhalam and J. W. Negele, Nucl. Phys. **A288**, 417 (1977).
[27]K. Goeke, A. Faessler, and H. H. Wolter, Nucl. Phys. **A183**, 352 (1972).